Massive Symmetry Breaking in $LaAlO_3/SrTiO_3(111)$ Quantum Wells: A Three-Orbital Strongly Correlated Generalization of Graphene

David Doennig,[1] Warren E. Pickett,[2] and Rossitza Pentcheva[1,*]

[1]*Department of Earth and Environmental Sciences, Section Crystallography and Center of Nanoscience, University of Munich, Theresienstrasse 41, 80333 Munich, Germany*

[2]*Department of Physics, University of California Davis, One Shields Avenue, Davis, California 95616, USA*

(Received 29 March 2013; published 19 September 2013)

Density functional theory calculations with an on-site Coulomb repulsion term reveal competing ground states in (111)-oriented $(LaAlO_3)_M/(SrTiO_3)_N$ superlattices with n-type interfaces, ranging from spin, orbitally polarized (with selective e_g', a_{1g}, or d_{xy} occupation), Dirac point Fermi surface, to charge-ordered flat band phases. These phases are steered by the interplay of (i) Hubbard U, (ii) $SrTiO_3$ quantum well thickness, and (iii) crystal field splitting tied to in-plane strain. In the honeycomb lattice bilayer $N = 2$ under tensile strain, inversion symmetry breaking drives the system from a ferromagnetic Dirac point (massless Weyl semimetal) to a charge-ordered multiferroic (ferromagnetic and ferroelectric) flat band massive (insulating) phase. With increasing $SrTiO_3$ quantum well thickness an insulator-to-metal transition occurs.

DOI: 10.1103/PhysRevLett.111.126804 PACS numbers: 73.21.Fg, 73.22.Gk, 75.70.Cn

Remarkably rich electronic behavior has been discovered at oxide interfaces ranging from two-dimensional conductivity, superconductivity, and magnetism to confinement induced and gate controlled metal-to-insulator transitions [1]. Most of the interest so far has been directed at (001) oriented interfaces as, e.g., the ones between the two band insulators $LaAlO_3$ (LAO) and $SrTiO_3$ (STO) [2–6]. Recently the growth and initial characterization, including the finding of a high mobility electron gas, of LAO films on STO(111) has been reported [7]. In contrast to the (001) direction where in the perovskite structure AO and BO_2 layers alternate, the (111) orientation comprises alternating stacking of AO_3 and B layers that can be highly charged: for example, $(LaO_3)^{3-}/Al^{3+}$ for LAO, $(SrO_3)^{4-}/Ti^{4+}$ for STO, as illustrated in Fig. 1(a). Despite the difference in stacking and charge of the individual layers, a polar discontinuity arises for both orientations, with a mismatch of $e/2$ per B cation for the n-type interfaces. For the (001) orientation this polar discontinuity is considered to be the origin of the rich spectrum of functional properties mentioned above, albeit the latter can also be influenced by defects. It is timely to investigate whether similar electronic reconstructions and exotic phases arise for the (111) orientation.

Perovskite (111) layers have a distinctive real space topology: each BO_6 layer constitutes a triangular lattice where the B cations are second neighbors. Combining two such layers in a bilayer forms a buckled honeycomb lattice, topologically equivalent to that of graphene [see Fig. 1(b)]; three layers form the also distinctive dice lattice. The possibility for a nontrivial topology of electrons hopping on a honeycomb lattice proposed by Haldane [8] has spurred model Hamiltonian studies of topologically nontrivial states for (111)-oriented perovskite superlattices [9–11], where the focus was on the $LaNiO_3$ (LNO) e_g system confined within LAO with quadratic band touching points, and a Dirac point at higher band filling [10–12]. This two-orbital honeycomb lattice is beginning to be grown and characterized [13,14].

The corresponding three-orbital t_{2g} system is realized for bilayer STO confined in LAO, where $e/2$ charge from each n-type "interface" (IF) will force one electron into 12 Ti conduction states (2 atoms, 3 orbitals, 2 spins), initially with $P321$ symmetry with two generators [threefold rotation; $(y, x, \bar{z})$, which we heuristically refer to as inversion]. The result is a 12-band, potentially strongly correlated generalization of graphene subject to numerous symmetry breaking possibilities: charge, spin, orbital, rotation, inversion $\mathcal{I}$, time reversal $\mathcal{T}$, and gauge symmetry; our methods

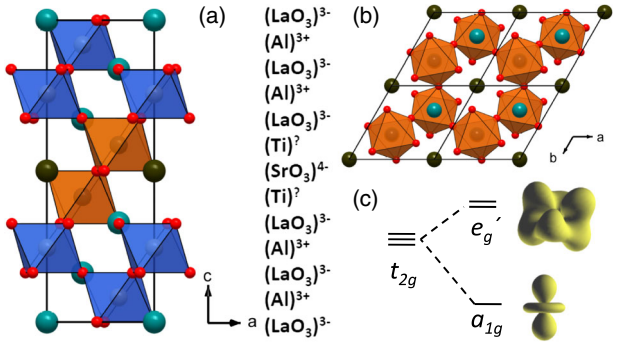

FIG. 1 (color online). (a) Side view of $(LAO)_4/(STO)_2(111)$ superlattice (SL) with an n-type interface. (b) Top view of the STO bilayer forming a buckled honeycomb lattice out of the two triangular lattices of Ti cations at each interface where the Ti are second nearest neighbors. (c) Splitting of the t_{2g} orbitals in a_{1g} and e_g' due to trigonal symmetry; relative sequence depends on strain.

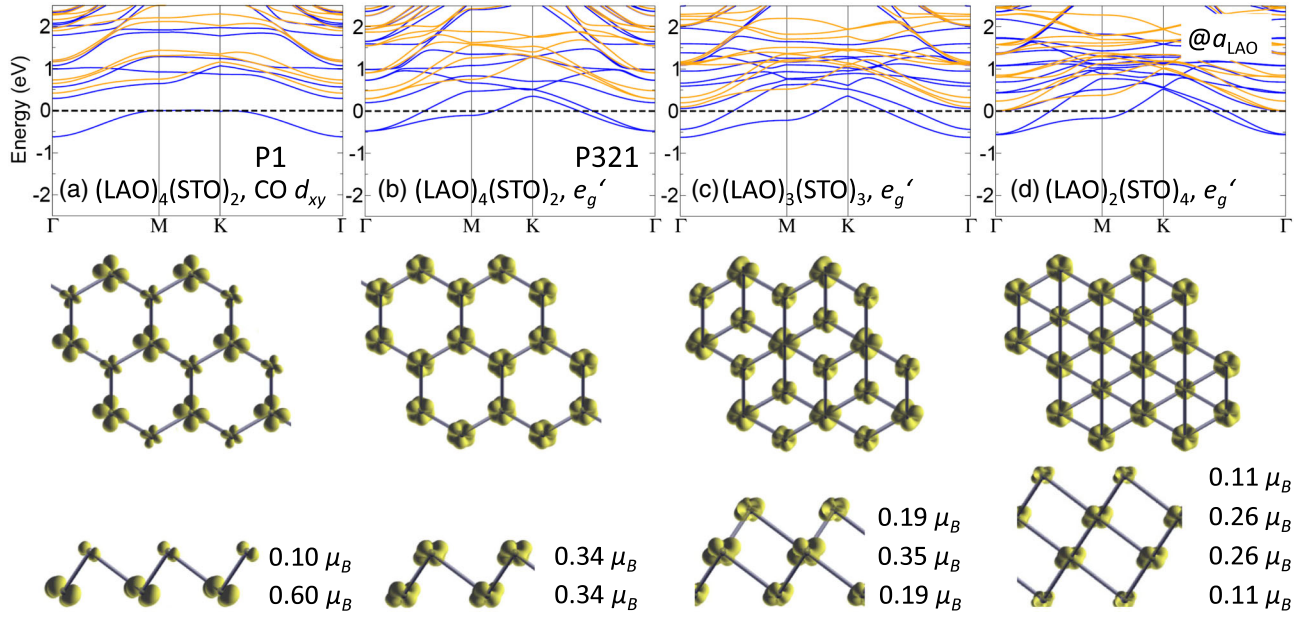

FIG. 2 (color online). Band structure and electron density distribution (top and side view), integrated over occupied Ti $3d$ bands, for $(\mathrm{LAO})_M/(\mathrm{STO})_N(111)$ superlattices at a_{LAO}. Majority and minority bands are plotted in blue (dark gray) and orange (light gray), respectively. (a) $N = 2$ charge-ordered FM insulator. Note the d_{xy} occupation, i.e., single real t_{2g} orbital. (b)–(d) $N = 2$, 3, 4 STO layers, retaining inversion symmetry with e_g' orbital occupation. For the thicker SLs ($N = 3$, 4) the excess charge is redistributed from the interface Ti layer to the central layers, a quantum confinement effect, and the band dispersion at Γ increases somewhat.

do not address the latter. The corresponding model Hamiltonian would include the symmetry group $\mathrm{SU}(2)_{\mathrm{spin}} \times \mathrm{SU}(2)_{\mathrm{orb}} \times P3 \times \mathcal{I} \times \mathcal{T} \times \mathrm{U}(1)_{\mathrm{gauge}}$.

A key question is that of orbital polarization, which is a primary factor in magnetic, transport, and optical properties. The geometry of the 111-superlattice breaks orbital threefold (t_{2g}) symmetry into trigonal $t_{2g} \rightarrow e_g' + a_{1g}$ as shown schematically in Fig. 1(c). For the (001) IF, previous density functional theory (DFT) studies predicted [15–18], and x-ray absorption spectroscopy data [19] demonstrated, that the t_{2g} degeneracy is lifted such that the d_{xy} orbital at the interface lies lower in energy. Including static local correlation effects within GGA + U (generalized gradient approximation plus Hubbard U method) stabilizes a charge-ordered and orbitally polarized layer with alternating Ti^{3+} and Ti^{4+} in the interface layer and a d_{xy} orbital occupied at the Ti^{3+} sites [15,16]. It will be instructive to compare this scenario with the behavior for the (111) orientation.

A mathematically symmetric expression adapted to trigonal symmetry for t_{2g} orbitals is

$$|\psi_m\rangle = (\zeta_m^0|d_{xy}\rangle + \zeta_m^1|d_{yz}\rangle + \zeta_m^2|d_{xz}\rangle)/\sqrt{3},$$

where $\zeta_m = e^{2\pi i m/3}$. One issue is whether complex e_g' orbitals $m = \pm 1$ ($m = 0$ is the a_{1g} orbital) assert themselves, inviting an anomalously large response to spin-orbit coupling in t_{2g} systems [20,21], or whether real combinations of the e_g' orbitals persist. Complex orbitals in the e_g bilayer have been predicted to encourage topological phases [12]. In this Letter we find that trigonal level splitting, which is directly connected to strain, determines the orbital occupation that vastly influences the electronic structure in the (111)-oriented STO quantum well (QW).

DFT calculations have been performed on $(\mathrm{LAO})_M/(\mathrm{STO})_N(111)$ superlattices with varying thickness M, N of both constituents, using the all-electron full-potential (FP) linearized augmented-plane-wave (LAPW) method, as implemented in the WIEN2k code [22,23]. The LAO thickness M is always large enough to confine the carriers to STO. Static local electronic correlations were added to the GGA exchange correlation potential [24] in the GGA + U method [25] with $U = 5$ eV, $J = 0.7$ eV (Ti $3d$), $U = 8$ eV (La $4f$). Values ranging between $U = 3$–8 have been used previously for oxides containing Ti^{3+} ($3d^1$) [15–17,26–28]. As discussed in the Supplemental Material [29], the obtained solutions are found to be robust with respect to variations of the on-site Coulomb repulsion parameter beyond $U = 2$ eV. The influence of strain was investigated by choosing the lateral lattice parameter of either LAO ($a_{\mathrm{LAO}} = 3.79$ Å) or STO ($a_{\mathrm{STO}}^{\mathrm{GGA}} = 3.92$ Å), which correspond to superlattices grown either on a LAO(111) or STO(111) substrate. We note that these lateral lattice constants impose different strain states in the two parts of the superlattice. The out-of-plane lattice parameter c was chosen to conserve the volume. For a_{LAO} the optimized c almost coincides with this value; however, an unexpectedly large c value was obtained for a_{STO}, similar to results for nickelate superlattices [30]. Octahedral tilts and distortions were fully taken into

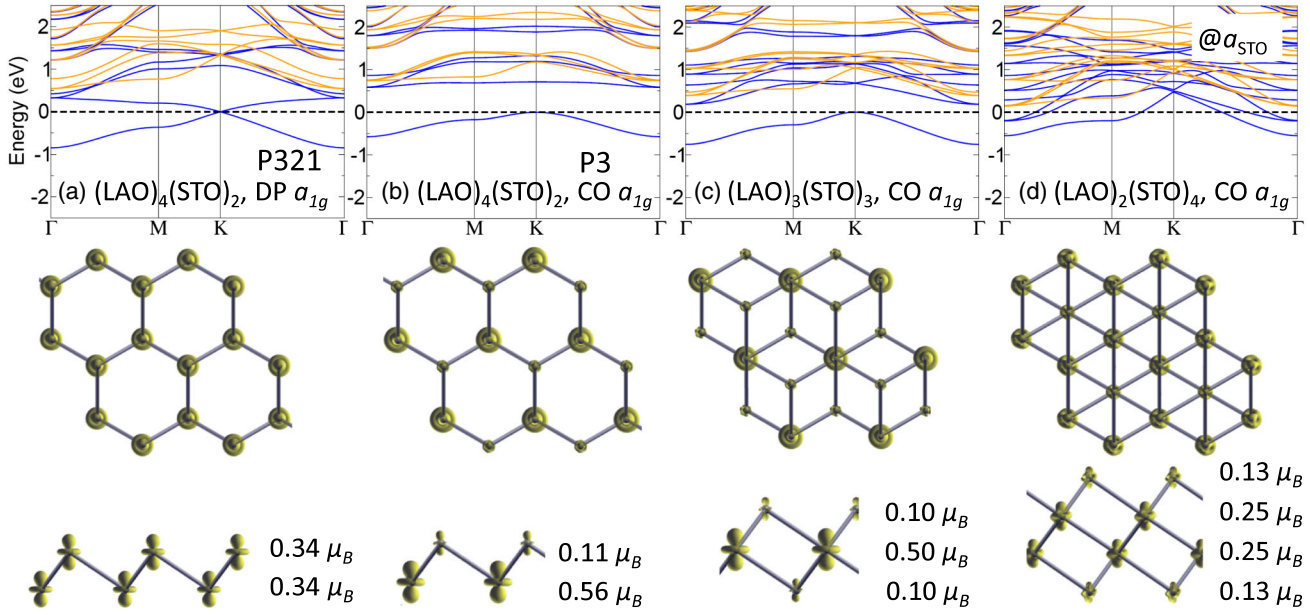

FIG. 3 (color online). As in Fig. 2, but for the superlattices at a_{STO}. Note the a_{1g} occupation independent of N. (a)–(b) $N = 2$. For the inversion symmetric interfaces (a) the system is a Weyl semimetal with Dirac points (DP) at K, K' as in graphene. (b) Allowing breaking of inversion symmetry results in inequivalent interfaces, Ti^{3+} versus Ti^{4+}, leading to the formation of a (111) dipole layer and insulating behavior. (c)–(d) With increasing STO thickness N the system switches from insulating ($N = 3$) to conducting behavior ($N = 4$).

account when relaxing atomic positions, whether constrained to $P321$ symmetry (threefold rotation plus $\mathcal{I}$) or fully released to $P1$ symmetry (in most cases solutions retained the higher $P3$ symmetry).

Results for a_{LAO}, corresponding to an underlying LAO (111) substrate.—Figure 2 presents results for n-type (111)-oriented $(\mathrm{LAO})_M/(\mathrm{STO})_N$ superlattices with thicknesses $N = 2$–4 of the STO quantum well, each of which is ferromagnetic (FM). The bilayer at a_{LAO} [see Fig. 2(a)] is a charge-ordered (CO) FM insulator with two distinct interfaces with Ti^{3+} $(0.60\mu_B)$ and Ti^{4+} $(0.10\mu_B)$, respectively, and due to broken inversion symmetry it is also ferroelectric (FE). The occupied orbital assumes local d_{xy} orientation [similar to the (001) superlattices [15–19]]. This state ($P1$ symmetry) is preferred by 120 meV/Ti over the inversion symmetric case [$P321$ symmetry, see Fig. 2(b)], where in contrast e_g' orbitals become preferentially occupied, indicating strong competition of electronic states with distinct orbital occupation, with very different symmetries, and electronic properties (ungapped versus gapped). e_g' orbital occupation is preferred also for $N = 3$ and 4 [see Figs. 2(c) and 2(d)] [31]. The difference in electronic structure for $N = 2$–4 [see Figs. 2(b)–2(d)] seems minor: the flattish lower conduction band is mostly occupied, leaving a hole Fermi surface (FS) surrounding the zone corner point K, with charge being balanced by one or two electron FS pockets centered at Γ. For the thicker $N = 3$, 4 STO QWs, the extra $e/2$ charge from each interface is distributed preferentially towards the central layers, related to the different chemical environment of interface versus central Ti ions.

Results for a_{STO}, corresponding to an underlying STO (111) substrate.—Using the in-plane STO lattice constant strains the LAO layer but leaves STO unstrained (subject to relaxation). A remarkably strong strain effect is the reversal of orbital polarization and the concomitant richer behavior: the symmetric a_{1g} orbital becomes occupied independent of the N_{STO} thickness, as shown in Fig. 3 (only for $N = 4$ the shape is distorted). Similar to the compressive case, the charge is shifted from the interface towards the central layers with increasing STO thickness. For the FM CO insulating $N = 2$ case, the top of the gap is bounded by a remarkably flat band. For the dice lattice (3/3) case the Ti^{3+} central layer $(0.50\mu_B)$ is sandwiched by Ti^{4+} interface layers, a confinement effect resulting in a FM insulating ground state. An insulator-to-metal transition occurs at $N = 4$, always retaining FM order, although the exchange splitting is reduced with increasing STO QW width. For LAO layers grown on STO(111), Herranz *et al.* found a critical thickness of ~10–12 LAO layers for the onset of conductivity, but their setup [7] is not comparable to the present QW system. We note from both Figs. 2 and 3 the proclivity of linear "Dirac" bands to occur at K, but when such points are not pinned to E_F they have no consequence.

As mentioned, the case $N = 2$ is special because the Ti bilayer forms a buckled honeycomb lattice, prompting us to study this system in more detail. The single electron can be shared equally and symmetrically by the two Ti ions, or

it can tip the balance to charge order, which requires symmetry breaking from $P321$ to $P3$ or possibly $P1$. Both CO and non-CO scenarios can be handled with or without other broken symmetries. We remind that in this t_{2g} system we always find that the spin symmetry is broken to FM order, regardless of in-plane strain, restriction of symmetry, and starting configuration. Similarly, in their model studies of an e_g bilayer honeycomb lattice (LNO superlattices), Rüegg *et al.* [12] found FM ordering for broad ranges of model parameters.

Constrained to $P321$ symmetry, a graphenelike Dirac point emerges at the zone corner point K that is pinned to the Fermi level and protected by the equivalence of the Ti sites [see Fig. 3(a)]. True particle-hole symmetry is restricted to relatively low energy due to coupling of the upper band to high-lying bands. The occupied bandwidth corresponds to hopping $t_{a_{1g},a_{1g}} = 0.28$ eV. Having a single electron shared symmetrically by two Ti sites is potentially unstable. Breaking of the equivalence of the Ti ions, i.e., $\mathcal{I}$ symmetry, results in a massless-to-massive transformation of the spectrum to a CO, FM, FE, and insulating state evident from Fig. 3(b) that is 95 meV/Ti more stable. Nearly complete charge disproportionation gives $Ti^{3+}(0.56\ \mu_B)$ and $Ti^{4+}(0.11\ \mu_B)$ alternating around each honeycomb hexagon, retaining the $P3$ symmetry, unlike the charge and orbitally ordered state for compressive strain ($P1$ symmetry).

In both cases [see Figs. 2(a) and 3(b)] charge ordering is accompanied by formation of an electric dipole in the bilayer as well as Ti-O bond alternation: in the latter tensile case the Ti-Ti interlayer distance is 2.1 Å, with a Ti^{4+}-O (Ti^{3+}-O) distance of 1.91 Å (1.98 Å), respectively (being 1.94 Å in the symmetric case). The orbital polarization, which is pure a_{1g} occupation, is distinct from the CO state for compressive strain, which has d_{xy} character; however these CO states compete at the larger optimized c lattice parameter. This aspect will be discussed in more detail in a future publication.

The occupied bandwidths and shapes of the CO states for the two strain states are very similar, and in each case the gap of ~0.8 eV leads to a higher-lying remarkably flat band [see Fig. 3(b)], which for tensile strain forms the bottom of the conduction band into which doped electrons would go. Nearly flat bands are interesting in the context of the fractional quantum Hall effect. Flat bands have been obtained in a variety of cases: from a d-p_x-p_y square lattice model [32] and from a p_x, p_y honeycomb lattice model [33]; Xiao *et al.* [9] and Fiete and collaborators [12,34] found that perfectly flat bands emerge also in an e_g bilayer model, and Rüegg *et al.* demonstrated [12] that they arise from strictly localized eigenstates with symmetric orbital ordering. Several other examples have been discovered and studied [35–40].

The band structure we obtain is qualitatively different from the case of LNO (e_g) superlattices where the states close to the Fermi level consist of four bands: two linearly crossing and two flat bands with a quadratic touching point at Γ [11,12]. In contrast, for this t_{2g} system at low filling there are only two relevant bands, and inversion symmetry breaking gaps the two linearly crossing bands into two relatively flat ones. The very flat conduction band we find occurs only for the CO states (which are the ground states) that involve either a_{1g} and d_{xy} orbital occupation, depending on strain.

Allowing a difference in on-site $3d$ energies will be an essential part of breaking $\mathcal{I}$ symmetry when modeling the transition from massless Dirac pair into massive (gapped) bands [see Figs. 3(a) and 3(b)]. This difference in Ti^{4+} and Ti^{3+} $3d$ energies will be similar to the $2p$ core level difference arising from different Ti-oxygen bond lengths, which is 1.7 eV, twice the occupied bandwidth of the Dirac band structure. Focusing on the majority (blue) bands of the CO state, a regularity can be seen: there is a parallel pair of bands of the same shape as the occupied band, but lying 1.3 eV higher, which is the pair of Ti^{3+} e_g' bands. Mirroring the flat band and again 1.3 eV higher are two more (no longer precisely) flat bands; these are the Ti^{4+} a_{1g} and e_g' bands.

As our analysis shows (see the Supplemental Material [29]), both the Dirac point and the charge-ordered state result from on-site correlation. Both solutions emerge at relatively small U values (1–2 eV) and are robust with respect to further increase of U. In the CO case, the primary effect of U is to encourage integer orbital occupations, i.e., a Mott insulating state: four quarter-filled spin orbitals (two sites, two orbitals) convert by CO to one empty sublattice and one half-filled sublattice, which then becomes Mott-insulating. This charge-ordered–Mott-insulator transition is driven by a combination of Hubbard U and symmetry breaking (accompanied by a substantial oxygen relaxation), and may be aided by intersite repulsion.

Bands on the same graphene lattice, displaying the topology that we find for the Dirac bilayer, have been related to topological character [9–11]. Typically topological phases are protected by time reversal symmetry coupled with additional symmetries. Fu [41] and others [42,43] have noted that SOC is not required, demonstrating that topological band insulators can also be protected by crystalline symmetry rather than $\mathcal{T}$ symmetry.

Now we summarize. Unexpected richness has been uncovered in (111)-oriented $LaAlO_3/SrTiO_3$ heterostructures, where carriers must reside in Ti t_{2g} states. The competing ground states are ferromagnetic, with strain-controlled crystal field splitting $t_{2g} \rightarrow a_{1g} + e_g'$ promoting strain engineering of orbital polarization. For the system under tensile strain, a graphenelike Dirac point degeneracy survives as long as inversion symmetry of the bilayer is preserved. Allowing breaking of this symmetry results in charge ordering with a flat conduction band and multiferroic properties, again with orbital polarization

dependent on strain. Melting of the CO phase as temperature is raised, where several symmetries (and conductivity) are restored, should reveal very rich behavior.

R. P. acknowledges discussions with M. Rozenberg. R. P. and D. D. acknowledge financial support through the DFG SFB/TR80 and Grant No. h0721 for computational time at the Leibniz Rechenzentrum. W. E. P. was supported by U.S. Department of Energy Award No. DE-FG02-04ER46111.

*rossitzap@lmu.de

[1] H. Y. Hwang, Y. Iwasa, M. Kawasaki, B. Keimer, N. Nagaosa, and Y. Tokura, Nat. Mater. **11**, 103 (2012).
[2] M. Huijben, A. Brinkman, G. Koster, G. Rijnders, H. Hilgenkamp, and D. A. Blank, Adv. Mater. **21**, 1665 (2009).
[3] J. Mannhart and D. G. Schlom, Science **327**, 1607 (2010).
[4] R. Pentcheva and W. E. Pickett, J. Phys. Condens. Matter **22**, 043001 (2010).
[5] P. Zubko, S. Gariglio, M. Gabay, P. Ghosez, and J.-M. Triscone, Annu. Rev. Condens. Matter Phys. **2**, 141 (2011).
[6] R. Pentcheva, R. Arras, K. Otte, V. G. Ruiz, and W. E. Pickett, Phil. Trans. R. Soc. A **370**, 4904 (2012).
[7] G. Herranz, F. Sanchez, N. Dix, M. Scigaj, and J. Fontcuberta, Sci. Rep. **2**, 758 (2012).
[8] F. D. M. Haldane, Phys. Rev. Lett. **61**, 2015 (1988).
[9] D. Xiao, W. Zhu, Y. Ran, N. Nagaosa, and S. Okamoto, Nat. Commun. **2**, 596 (2011).
[10] A. Rüegg and G. A. Fiete, Phys. Rev. B **84**, 201103 (2011).
[11] K.-Y. Yang, W. Zhu, D. Xiao, S. Okamoto, Z. Wang, and Y. Ran, Phys. Rev. B **84**, 201104(R) (2011).
[12] A. Rüegg, C. Mitra, A. A. Demkov, and G. A. Fiete, Phys. Rev. B **85**, 245131 (2012).
[13] M. Gilbert, P. Zubko, R. Scherwitzl, and J.-M. Triscone, Nat. Mater. **11**, 195 (2012).
[14] S. Middey, D. Meyers, M. Kareev, E. J. Moon, B. A. Gray, X. Liu, J. W. Freeland, and J. Chakhalian, Appl. Phys. Lett. **101**, 261602 (2012).
[15] R. Pentcheva and W. E. Pickett, Phys. Rev. B **74**, 035112 (2006).
[16] R. Pentcheva and W. E. Pickett, Phys. Rev. B **78**, 205106 (2008).
[17] Z. Zhong and P. J. Kelly, Europhys. Lett. **84**, 27 001 (2008).
[18] Z. S. Popovic, S. Satpathy, and R. M. Martin, Phys. Rev. Lett. **101**, 256801 (2008).
[19] M. Salluzzo *et al.*, Phys. Rev. Lett. **102**, 166804 (2009).
[20] V. Pardo and W. E. Pickett, Phys. Rev. B **81**, 245117 (2010).
[21] V. Pardo and W. E. Pickett, Phys. Rev. B **81**, 035111 (2010).
[22] K. Schwarz and P. Blaha, Comput. Mater. Sci. **28**, 259 (2003).
[23] P. Blaha, K. Schwarz, G. K. H. Madsen, D. Kvasnicka, and J. Luitz, *WIEN2k, An Augmented Plane Wave Plus Local Orbitals Program for Calculating Crystal Properties* (Vienna University of Technology, Vienna, Austria, 2001).
[24] J. P. Perdew, K. Burke, and M. Ernzerhof, Phys. Rev. Lett. **77**, 3865 (1996).
[25] V. I. Anisimov, J. Zaanen, and O. K. Andersen, Phys. Rev. B **44**, 943 (1991).
[26] I. Solovyev, N. Hamada, and K. Terakura, Phys. Rev. B **53**, 7158 (1996).
[27] E. Pavarini, S. Biermann, A. Poteryaev, A. Lichtenstein, A. Georges, and O. Andersen, Phys. Rev. Lett. **92**, 176403 (2004).
[28] S. V. Streltsov, A. Mylnikova, A. Shorikov, Z. Pchelkina, D. Khomskii, and V. Anisimov, Phys. Rev. B **71**, 245114 (2005).
[29] See Supplemental Material at http://link.aps.org/supplemental/10.1103/PhysRevLett.111.126804 for details on lattice relaxations and dependence on U.
[30] J. W. Freeland, J. Liu, M. Kareev, B. Gray, J. W. Kim, P. Ryan, R. Pentcheva, and J. Chakhalian, Europhys. Lett. **96**, 57 004 (2011).
[31] The orbital polarization is quenched to t_{2g} only for strong compression of the c lattice constant.
[32] K. Sun, Z. Gu, H. Katsura, and S. Das Sarma, Phys. Rev. Lett. **106**, 236803 (2011).
[33] C. Wu, D. Bergman, L. Balents, and S. Das Sarma, Phys. Rev. Lett. **99**, 070401 (2007).
[34] X. Hu, A. Rüegg, and G. A. Fiete, Phys. Rev. B **86**, 235141 (2012).
[35] D. L. Bergman, C. Wu, and L. Balents, Phys. Rev. B **78**, 125104 (2008).
[36] C. Weeks and M. Franz, Phys. Rev. B **85**, 041104 (2012).
[37] F. Wang and Y. Ran, Phys. Rev. B **84**, 241103 (2011).
[38] J.-M. Hou, Commun. Theor. Phys. **52**, 247 (2009).
[39] D. Green, L. Santos, and C. Chamon, Phys. Rev. B **82**, 075104 (2010).
[40] H. Katsura, I. Maruyama, A. Tanaka, and H. Tasaki, Europhys. Lett. **91**, 57 007 (2010).
[41] L. Fu, Phys. Rev. Lett. **106**, 106802 (2011).
[42] M. Kargarian and G. A. Fiete, Phys. Rev. Lett. **110**, 156403 (2013).
[43] R.-J. Slager, A. Mesaros, V. Juricic, and J. Zaanen, Nat. Phys. **9**, 98 (2013).